Validation of buoyancy driven spectral tensor model using HATS data

Chougule, A.; Mann, Jakob; Kelly, Mark C.; Larsen, Gunner Chr.

Published in:
Journal of Physics: Conference Series (Online)

Link to article, DOI:
10.1088/1742-6596/753/3/032038

Publication date:
2016

Document Version
Publisher's PDF, also known as Version of record

Validation of buoyancy driven spectral tensor model using HATS data

2016 J. Phys.: Conf. Ser. 753 032038

(http://iopscience.iop.org/1742-6596/753/3/032038)

Validation of buoyancy driven spectral tensor model using HATS data

A Chougule[1], J Mann[2], M Kelly[2] and G C Larsen[2]
[1]Department of Engineering Sciences, University of Agder, 4879 Grimstad, Norway
[2]DTU Wind Energy, Technical University of Denmark, 4000 Roskilde, Denmark

E-mail: abhijit.chougule@uia.no

Abstract. We present a homogeneous spectral tensor model for wind velocity and temperature fluctuations, driven by mean vertical shear and mean temperature gradient. Results from the model, including one-dimensional velocity and temperature spectra and the associated co-spectra, are shown in this paper. The model also reproduces two-point statistics, such as coherence and phases, via cross-spectra between two points separated in space. Model results are compared with observations from the Horizontal Array Turbulence Study (HATS) field program (Horst et al. 2004). The spectral velocity tensor in the model is described via five parameters: the dissipation rate (ϵ), length scale of energy-containing eddies (L), a turbulence anisotropy parameter (Γ), gradient Richardson number (Ri) representing the atmospheric stability and the rate of destruction of temperature variance (η_θ).

1. Introduction

Modeling of the spectral velocity tensor has important implications in wind energy. The International Electrotechnical Commission [1] recommends the use of the three-dimensional spectral tensor model by Mann [2] for estimation of loads on wind turbines, through simulation of rotor inflow [3]. The examples of the other models which describes the spectra and cross-spectra could be, the models– developed by Kristensen et al. [4], Kaimal et al. [5], etc. The model by Mann [2] (hereafter denoted M94) differs from the other models mentioned above in many respects. It incorporates rapid distortion theory (RDT) [6, 7], with an assumption of uniform mean shear and a dedicated model for eddy life time. The stationary M94 model is applicable for homogeneous neutral surface-layer turbulence. RDT has previously been used in non-stationary spectral tensor modeling of homogeneous– uniform sheared [8], unsheared stably stratified [9], and sheared stably stratified [10, 11] turbulent flows. The M94 model contains three adjustable parameters which are determined from the single-point measurements. Although the model was never extended to account for buoyancy effects, it has been used to describe one-point spectra for non-neutral conditions in [12, 13, 14]. For the simulation of turbulence in the lower atmosphere and subsequent estimation of its loading effects upon structures, it would be useful to augment the M94 spectral tensor model, to include buoyancy effects.

This paper summarizes the present state of the model. In Section 2, we provide the basic definition of the spectral tensor, the governing RDT equations to the model, and the initial conditions as state of the isotropic turbulence. Section 3 provides the information about the HATS experiments and the data used for the model validation. The results from the modeling and observations are discussed in Section 4.

2. Spectral tensor model

In homogeneous turbulence, the spectral velocity tensor is defined as

$$\Phi_{ij}(\boldsymbol{k}) = \frac{1}{(2\pi)^3}\int R_{ij}(\boldsymbol{r})\mathrm{e}^{-\mathrm{i}\boldsymbol{k}\cdot\boldsymbol{r}}\mathrm{d}\boldsymbol{r}, \tag{1}$$

where $\boldsymbol{k} = (k_1, k_2, k_3)$ is the wavenumber vector, $R_{ij}(\boldsymbol{r})$ is the covariance tensor with separation distance $\boldsymbol{r}$, and $\int \mathrm{d}\boldsymbol{r} \equiv \int_{-\infty}^{\infty}\int_{-\infty}^{\infty}\int_{-\infty}^{\infty}\mathrm{d}r_1\mathrm{d}r_2\mathrm{d}r_3$.

The two-point correlations of the Fourier velocity components are related to the spectral tensor by

$$\frac{\langle \mathrm{d}Z_i^*(\boldsymbol{k})\mathrm{d}Z_j(\boldsymbol{k})\rangle}{\mathrm{d}k_1\mathrm{d}k_2\mathrm{d}k_3} = \Phi_{ij}(\boldsymbol{k}), \tag{2}$$

where $\langle\ \rangle$ denotes ensemble average operator; the superscript $*$ denotes complex conjugate. The spectral representation of the three-dimensional fluctuating velocity field $\boldsymbol{u}'(\boldsymbol{x}, t)$, to be considered as non-periodic, can be given in terms of the Fourier-Stieltjes integral

$$\boldsymbol{u}'(\boldsymbol{x}) = \int \mathrm{e}^{\mathrm{i}\boldsymbol{k}\cdot\boldsymbol{x}}\mathrm{d}\boldsymbol{Z}(\boldsymbol{k}), \tag{3}$$

where the integration in (3) is over all wavenumber space [15].

2.1. Governing equations

The spectral tensor is modeled using (2), where the equation for the evolution of the Fourier modes $\mathrm{d}\boldsymbol{Z}(\boldsymbol{k}, t)$ will be deduced from the governing Navier-Stokes equations (NSE) via RDT given as,

$$\frac{\mathrm{D}}{\mathrm{D}\xi}\mathrm{d}Z_l(\boldsymbol{k}(\xi), \xi) = \mathrm{M}_{lm}(\boldsymbol{k}(\xi), \xi)\mathrm{d}Z_m(\boldsymbol{k}(\xi), \xi), \tag{4}$$

where $l, m = 1, 2, 3, 4$;

$$\mathrm{M}_{lm}(\boldsymbol{k}(\xi), \xi) = \begin{pmatrix} 0 & 0 & \frac{2k_1^2}{k^2} - 1 & -\frac{k_1k_3}{k^2} \\ 0 & 0 & \frac{2k_1k_2}{k^2} & -\frac{k_2k_3}{k^2} \\ 0 & 0 & \frac{2k_1k_3}{k^2} & -\left(\frac{k_3^2}{k^2} - 1\right) \\ 0 & 0 & -\mathrm{Ri} & 0 \end{pmatrix}; \tag{5}$$

and, the Richardson number Ri, defined as [16]

$$\mathrm{Ri} = \left(\frac{g}{\overline{\theta}}\right)\frac{\mathrm{d}\overline{\theta}/\mathrm{d}z}{(\mathrm{d}U/\mathrm{d}z)^2}. \tag{6}$$

We use non-dimensional time $\xi = (\mathrm{d}U/\mathrm{d}z)t$. The rate of change of wavenumber due to mean shear becomes

$$\frac{\mathrm{d}k_3}{\mathrm{d}t} = -k_1\frac{\mathrm{d}U}{\mathrm{d}z}, \tag{7}$$

with the mean velocity field considered as $(U, 0, 0)$. We represent the potential temperature θ (hereafter temperature) by a new quantity, defined as

$$\mathrm{d}Z_4(\boldsymbol{k}(t), t) = \frac{g}{\overline{\theta}}\left(\frac{\mathrm{d}U}{\mathrm{d}z}\right)^{-1}\mathrm{d}\Theta(\boldsymbol{k}(t), t), \tag{8}$$

where $\mathrm{d}\Theta(\boldsymbol{k}(t), t)$ is Fourier counterpart of temperature just as that given in (3), for velocity.

2.2. Initial conditions

We assume initial condition as the state of isotropic turbulence. For the velocity components, the isotropic tensor is given as [7]

$$\Phi_{ij}(\boldsymbol{k}_0, 0) = \frac{E(k)}{4\pi k^2}\left(\delta_{ij} - \frac{k_i k_j}{k^2}\right). \tag{9}$$

We use the form of the energy spectrum $E(k)$, given by von Kármán as

$$E(k) = \alpha\epsilon^{\frac{2}{3}}L^{\frac{5}{3}}\frac{(kL)^4}{(1+(kL)^2)^{\frac{17}{6}}}, \tag{10}$$

where ϵ is the rate of viscous dissipation of specific turbulent kinetic energy, L is a length scale and $\alpha \approx 1.7$ is the spectral Kolmogorov constant.

For temperature, the isotropic three-dimensional spectrum is given as

$$\Phi_{\theta\theta}(\boldsymbol{k}_0, 0) = \frac{S(k)}{4\pi k^2}, \tag{11}$$

where $S(k)$ is the potential energy spectrum containing the form of the inertial subrange [16] as,

$$S(k) = \beta_1\epsilon^{-1/3}\epsilon_\theta L^{\frac{5}{3}}\frac{(kL)^2}{(1+(kL)^2)^{\frac{11}{6}}}, \tag{12}$$

where ϵ_θ is the dissipation rate for half the temperature variance and $\beta_1 = 0.8$ is a universal constant [5]. From equations (8), (11), and (12),

$$\Phi_{44}(\boldsymbol{k}_0, 0) = \frac{S'(k)}{4\pi k^2}, \tag{13}$$

where

$$S'(k) = \beta\eta_\theta\frac{1+(kL)^2}{(kL)^2}E(k), \tag{14}$$

$\beta = \beta_1/\alpha$, and

$$\eta_\theta = \frac{\epsilon_\theta}{\epsilon}\left[\frac{g}{\overline{\theta}}\left(\frac{\mathrm{d}U}{\mathrm{d}z}\right)^{-1}\right]^2. \tag{15}$$

From equation (4) and the definitions of $E(k)$ and $S'(k)$, the anisotropic tensor $\Phi(\boldsymbol{k}, \xi)$ can be expressed as,

$$\Phi(\boldsymbol{k}, \xi) \equiv \Phi(\boldsymbol{k}, \alpha\epsilon^{\frac{2}{3}}, L, \xi, \mathrm{Ri}, \beta\eta_\theta). \tag{16}$$

From (10)-(14), it can be proven that

$$\Phi(\boldsymbol{k}, \alpha\epsilon^{\frac{2}{3}}, L, \xi, \mathrm{Ri}, \beta\eta_\theta) = \alpha\epsilon^{\frac{2}{3}}L^{\frac{11}{3}}\Phi(\boldsymbol{k}L, 1, 1, \xi, \mathrm{Ri}, \beta\eta_\theta). \tag{17}$$

2.3. Stationarity

The spectral tensor in (17) is non-stationary (time-dependent, via ξ), and the stretching of eddies due to shear for an infinitely long time is unrealistic. The eddies must break at some point due to the stretching. The eddies will stretch or compress depending upon their orientation in the plane of uniform shear. In order to make the spectral tensor stationary, we incorporate the general concept of eddy life time from M94 and its parameterization

$$\tau(k) = \Gamma\left(\frac{\mathrm{d}U}{\mathrm{d}z}\right)^{-1}(kL)^{-2/3}\left[{}_2F_1\left(\frac{1}{3}, \frac{17}{6}; \frac{4}{3}; -(kL)^{-2}\right)\right]^{-1/2}, \tag{18}$$

where Γ is a parameter to be determined, and ${}_2F_1$ is the 'ordinary' or 'Gaussian' hypergeometric function. We make the spectral tensor in (17) stationary by replacing t in ξ with the wavenumber-dependent eddy life time given in (18), so $\xi \to \Gamma$ in the arguments of Φ, and the anisotropic spectral tensor becomes

$$\Phi(\boldsymbol{k}, \alpha\epsilon^{\frac{2}{3}}, L, \Gamma, \mathrm{Ri}, \beta\eta_\theta) = \alpha\epsilon^{\frac{2}{3}} L^{\frac{11}{3}} \Phi(\boldsymbol{k}L, 1, 1, \Gamma, \mathrm{Ri}, \beta\eta_\theta). \tag{19}$$

2.4. Model output

The model cross-spectrum between any two velocity components, or, between any velocity component and temperature, is given as

$$\chi_{ij}(k_1, \Delta y, \Delta z) = \int \Phi_{ij}(\boldsymbol{k}) \mathrm{e}^{\mathrm{i}(k_2\Delta y + k_3 \Delta z)} \mathrm{d}\boldsymbol{k}_\perp. \tag{20}$$

From the above equation and (19),

$$\chi_{ij}(k_1, \Delta y, \Delta z) = \alpha\epsilon^{\frac{2}{3}} L^{\frac{5}{3}} \int \Phi_{ij}(\boldsymbol{k}L, 1, 1, \Gamma, \mathrm{Ri}, \beta\eta_\theta) \mathrm{e}^{\mathrm{i}(k_2\Delta y + k_3 \Delta z)} \mathrm{d}\boldsymbol{k}_\perp L^2, \tag{21}$$

where $\int \mathrm{d}\boldsymbol{k}_\perp = \int_{-\infty}^{\infty}\int_{-\infty}^{\infty} \mathrm{d}k_2 \mathrm{d}k_3$. Δy and Δz are transverse and vertical separations, respectively. The model parameters at any height z, are obtained by fitting model one-dimensional spectra and co-spectra

$$F_{ij}(k_1) = \chi_{ij}(k_1, 0, 0), \tag{22}$$

with measured power-spectra (including co-spectra $uw, u\theta$ and $w\theta$).

The cross-spectral properties, the squared coherence and the cross-spectral phase, defined respectively as

$$\mathrm{coh}_{ij}(k_1, \Delta y, \Delta z) = \frac{|\chi_{ij}(k_1, \Delta y, \Delta z)|^2}{F_i(k_1) F_j(k_1)}, \tag{23}$$

$$\varphi_{ij}(k_1, \Delta y, \Delta z) = \arg(\chi_{ij}(k_1, \Delta y, \Delta z)). \tag{24}$$

For non-zero separations, the average of the parameters between two points are used as inputs to estimate the model coherence and phases.

3. Model validation

We validate our model using the observations from the HATS field program, which was carried out in September 2000 near Kettleman City, California [17].

3.1. HATS Experiment

A number of different setup configurations are deployed in the HATS experiment, where two horizontal arrays of sonic anemometers, each measuring temperature and three-dimensional wind velocity, are placed at different heights from the ground. As shown in figure 1, horizontal s-array of five sonic anemometers are placed at one height z_s from the ground, and nine sonics in d-array mounted at a second height z_d parallel to the s-array. The sonics in the horizontal s- and d-array are separated by S_s and S_d, respectively. More information about the HATS experiment can be found in [17, 18].

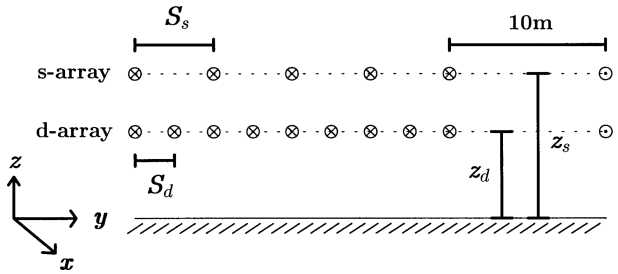

Figure 1: The HATS experimental setup: The sonic anemometers ⊗ are mounted vertically in the single and double array at (z_s, z_d) above the ground. Source: [17].

3.2. Method

We estimate the velocity spectra and co-spectrum of u and w from the measured time-series as

$$F_{ij}(f,z) \equiv \langle \hat{u}_i(f)\hat{u}_j^*(f)\rangle, \tag{25}$$

and the temperature spectrum and the component-wise kinematic heat fluxes, respectively as

$$F_\theta(f,z) \equiv \langle \hat{\theta}(f)\hat{\theta}^*(f)\rangle, \tag{26}$$

$$F_{i\theta}(f,z) \equiv \langle \hat{u}_i(f)\hat{\theta}^*(f)\rangle, \tag{27}$$

where $f = 20$ Hz is the frequency, $\hat{u}_i(f)$ and $\hat{\theta}(f)$ are the complex-valued Fourier transform of the ith velocity component and temperature, respectively at height z.

The atmospheric stability is measured in terms of the ratio z/L_o, where the Obukhov length L_o is defined as [16]

$$L_o = \frac{-{u_*}^3}{\kappa(g/T)\overline{w'T'}_0}, \tag{28}$$

where u_* is the surface friction velocity, $\kappa = 0.4$ is the von Kármán constant, T is the mean surface-layer temperature and $\overline{w'T'}_0$ is the vertical kinematic heat flux density at the surface.

We perform χ^2-fits [2] of the model to the measured power-spectra in equations (25)-(27) using Taylor's hypothesis: $k_1 = 2\pi f/U$, to obtain the five parameters (given in equation (19)). The basic idea of the χ^2-fit is to minimize the sum of the squared differences between the theoretical and the estimated spectra and co-spectra.

4. Results and discussion

We calculate the spectra and co-spectra from the middle sonics and cross-spectra between the sonics in s- and d-arrays, from thirty-minute time-series using above method.

4.1. Spectra

The measured velocity spectra and co-spectrum of uw (left graph), and the temperature spectrum and co-spectra of $u\theta$, and $w\theta$ (right graph), for $z/L_o = 0.08$ along with the model spectral fits are shown in figure 2, at $z = 5$ m.

The velocity and temperature spectra follows the power law in the inertial sub-range, i.e., $F(k_1) \propto k_1^{-5/3}$, whereas the slope of the uw and $w\theta$ curves follows $k_1^{-7/3}$ in the inertial sub-range both modeled and observed. However, the observed $u\theta$ co-spectrum for stable case decay much faster with a slope close to -3 than $w\theta$. Our model predicts a slope close to -3 in the $u\theta$ co-spectrum, which is consistent with the prediction by [19]. In contrast, [5] noted an averaged slope of $-5/2$ for stable cases.

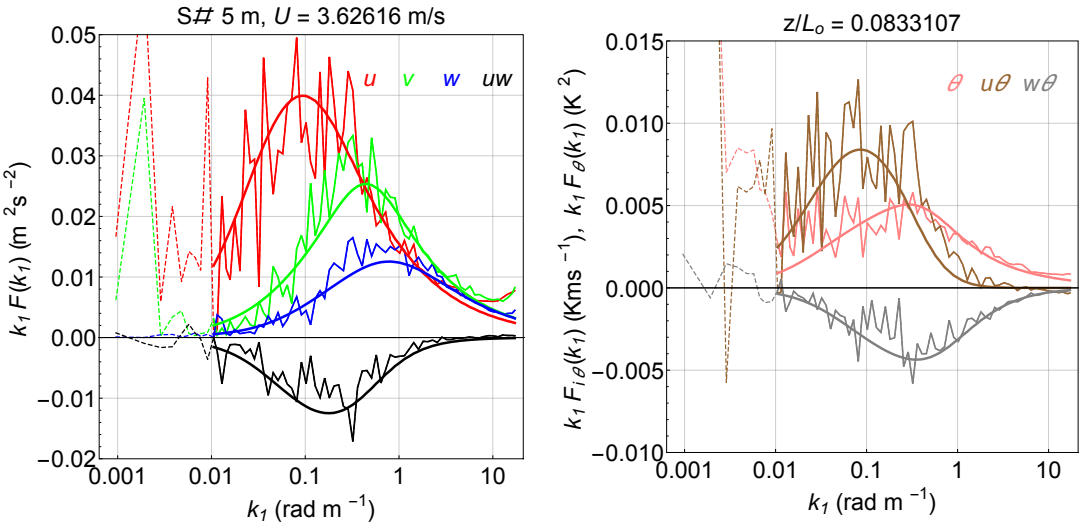

Figure 2: Model spectra and co-spectra (smooth lines) fitted with observations (ragged lines) at $z = 5$ m for $z/L_o = 0.08$.

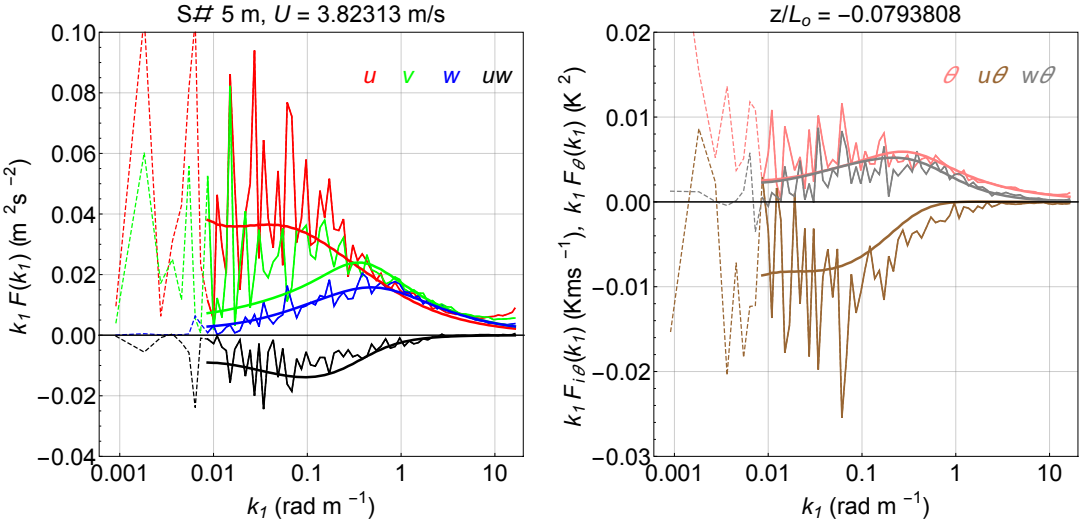

Figure 3: Model spectral fits to the measurements (ragged lines) at $z = 5$ m for $z/L_o = -0.08$.

The spectral fits from the model at 5 m, for unstable case: $z/L_o = -0.079$ are shown in figure 3. There is a sharp increase in the u-spectrum at lower wavenumbers in unstable case, which also causes an increase in the uw and $u\theta$ co-spectra at lower frequencies. Therefore we remove the low-frequency measured spectra (as shown by dotted lines in figure 3) during spectral fits and the five model parameters are obtained. A -3 slope of the $u\theta$ co-spectrum given by the model does not agree with the data for unstable case, where the data shows a slope close to $-7/3$. The five parameter values from the spectral fits that are shown in figure 2 and 3, are provided in Table 1.

Table 1: Five spectral tensor parameters determined from χ^2-fits for given stability z/L_o.

	Model Parameters				
z/L_o	$\alpha\epsilon^{2/3}$ ($m^{4/3}$ s^{-2})	L (m)	Γ	Ri	η_θ
0.08	0.09	2.9	3.7	0.035	0.005
-0.08	0.084	3.6	2.85	-0.04	0.01

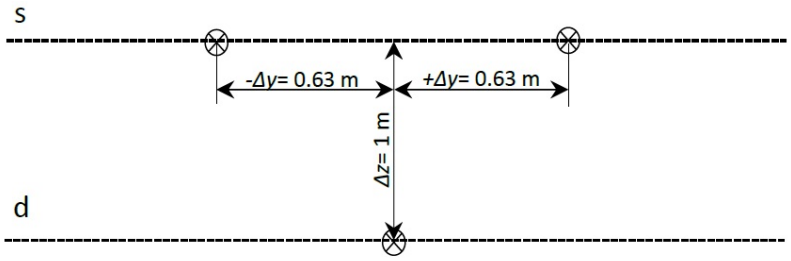

Figure 4: Sketch for the coherence calculations in figure 5. Coherences are calculated with respect to the middle sonic in the d-array for $(-\Delta y, \Delta z)$ and $(+\Delta y, \Delta z)$.

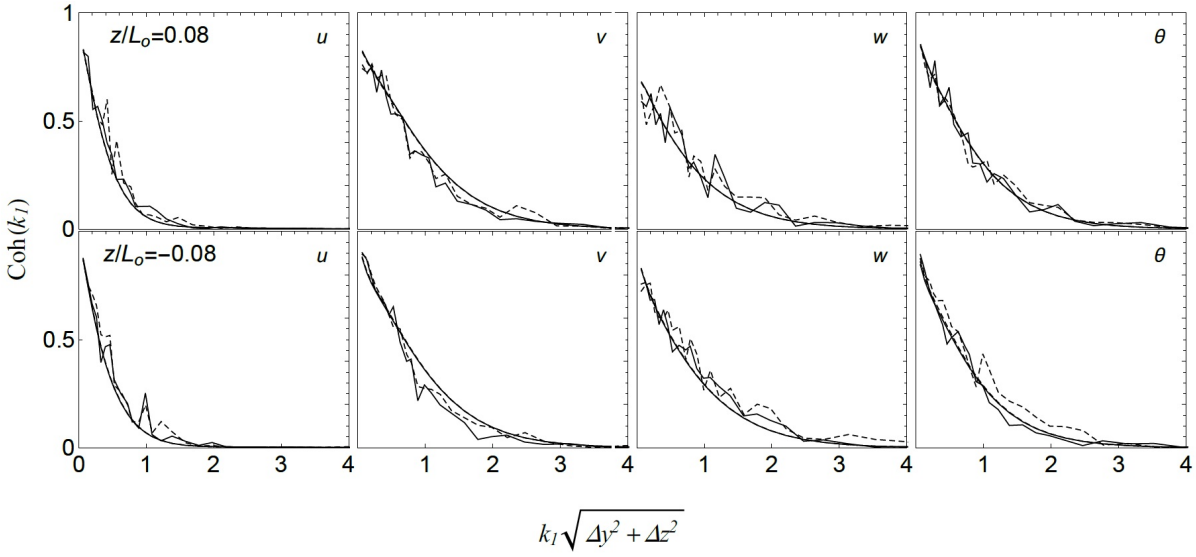

Figure 5: Model coherence (smooth lines) compared with observations (ragged lines), where $\pm\Delta y = 0.63$ m, $\Delta z = 1$ m for (a) $z/L_o = 0.08$, and (b) $z/L_o = -0.08$. Coherence for $(+\Delta y, \Delta z)$ are indicated by solid lines, whereas the dashed lines shows coherence for $(-\Delta y, \Delta z)$ separation.

4.2. Cross-spectra

Winds almost normal to the plane of arrays are selected, and the cross-spectra are rotated such that the mean velocity field is $(U, 0, 0)$, in order to compare results with the theory. The model coherences and cross-spectral phases are calculated using equations (23) and (24), respectively. The coherence for separation distances $(\pm\Delta y, \Delta z) = (0.63, 1)$ m between the sonics as shown in figure 4, are compared with the model results in figure 5, for both the positive and negative z/L_o's. The model has left-right symmetry, where the model coherence that are calculated with respect to the middle sonics in the d-array for $(-\Delta y, \Delta z)$ and $(+\Delta y, \Delta z)$ are equal. The

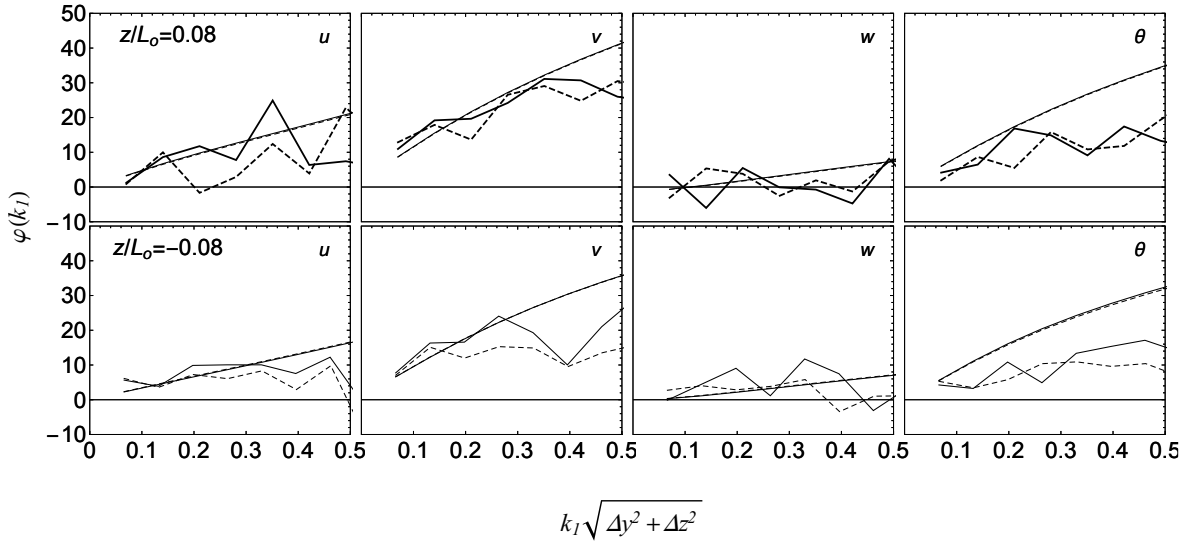

Figure 6: Model phases (smooth lines) compared with observations (ragged lines) for (a) $z/L_o = 0.08$, and (b) $z/L_o = -0.08$, with $\pm\Delta y = 0.63$ m, $\Delta z = 1$ m. Phases for $+\Delta y$ are indicated by solid lines, whereas the dashed lines shows phases for $-\Delta y$ separation.

observed coherence also show a pattern close to the symmetry. A horizontal-axis wind turbine in the free wind has its yaw motion such that the rotor plane is perpendicular to the mean wind direction grasping more energy in the mean wind field, whence the turbulent field may have left-right symmetry in the vertical plane of the rotor. For a wind turbine in the wake region, where due to the meandering effect, if the wind turbine subjected to the wake is not quick enough in its yaw motion, the turbulent field may no longer be symmetric in the lateral direction.

It is observed from figure 5 that the thermal stability has the most noticeable effect on the w-coherence which is larger in the unstable than the stable stratification, and the u-coherence is less affected by it. The phases in the modeled cross-spectra for the configuration given in figure 4, are compared with the observed phases in figure 6, both for stable and unstable stratification. It can be observed that φ_v (and φ_θ) $> \varphi_u > \varphi_w (\approx 0)$ [20]. There is no systematic effect of atmospheric stability on the phases [21]. Both the model and observed phases for horizontal separation are zero.

5. Conclusion

A spectral velocity tensor model including buoyancy via uniform vertical temperature gradient is validated with the atmospheric surface-layer data obtained from HATS. Using the χ^2-fit routine for parameter estimation, the model is able to reproduce velocity and temperature spectra and co-spectra $uw, u\theta$ and $w\theta$.

Our model predicts a slope closer to -3 for the $u\theta$ co-spectrum under stable and unstable stratification, consistent with the theoretical prediction by [19]. The data from stable stratification shows a slope closer to -3 in the $u\theta$ co-spectrum. In contrast to the situation for θ-spectrum and $w\theta$ co-spectrum, the slope of the unstable $u\theta$ co-spectrum does not agree with our prediction as the data shows a slope close to $-7/3$.

The data, from the coherence results, indicate the left-right symmetry inherent in the model. The phases in the modeled cross-spectra are compared with the observed phases which shows that the phase of temperature is larger than the phases in the streamwise and vertical velocity components, while the model is able to predict the trend which is φ_v and $\varphi_\theta > \varphi_u > \varphi_w (\approx 0)$.

Acknowledgements
This study is part of Norwegian Centre for Offshore Wind Energy (NORCOWE) under Grant 193821/S60 from Research Council of Norway (RCN). The EUDP project "Impact of atmospheric stability conditions on wind farm loading and production" under contract 64010-0462 is acknowledged for financial support to this study. We are also obliged to the COMWIND project funded by the Danish Council of Strategic Research (DSF-contract: 09-067216).

References
[1] IEC 2005 Wind turbines - part 1: Design requirements Tech. Rep. IEC 61400-1
[2] Mann J 1994 *J. Fluid Mech.* **273** 141–168
[3] Mann J 1998 *Prob. Engng. Mech.* **13(4)** 269–282
[4] Kristensen L, Lenschow D H, Kirkegaard P and Courtney M 1989 *Bound. Layer Meteorol.* **47** 149–193
[5] Kaimal J C, Wyngaard J C, Izumi Y and Coté O R 1972 *Quart. J. R. Met. Soc.* **98** 563–589
[6] Townsend A A 1976 *The structure of turbulent shear flow* 2nd ed (UK: Cambridge University Press)
[7] Pope S B 2000 *Turbulent flows* 1st ed (UK: Cambridge University Press)
[8] Maxey M R 1982 *J. Fluid Mech.* **124** 261–282
[9] Hanazaki H and Hunt J C R 1996 *J. Fluid Mech.* **318** 303–337
[10] Hanazaki H and Hunt J C R 2004 *J. Fluid Mech.* **507** 1–42
[11] Segalini A and Arnqvist J 2015 *J. Fluid. Mech.* **781** 330–352
[12] Peña A, Gryning S and Mann J 2010 *Q. J. R. Meteorol. Soc.* **136** 2119–2131
[13] Peña A, Gryning S, Mann J and Hasager C B 2010 *J. Appl. Meteor. Climat.* **49** 792–806
[14] Sathe A, Mann J, Barlas T, Bierbooms W A A M and van Bussel G J W 2012 *Wind Energy* **16** 1013–1032
[15] Batchelor G K 1953 *The theory of homogeneous turbulence* (UK: Cambridge University Press)
[16] Kaimal J C and Finnigan J J 1994 *Atmospheric boundary layer flows* (New York: Oxford University Press)
[17] Horst T W, Kleissl J, Lenschow D H, Meneveau C, Moeng C H, Parlange M B, Sullivan P P and Weil J C 2004 *J Atmos. Sci.* **61** 1566–1581
[18] Sullivan P P, Horst T W, Lenschow D H, Moeng C and Weil J C 2003 *J. Fluid Mech.* **482** 101–139
[19] Wyngaard J C and Coté O R 1972 *Quart. J. R. Met. Soc.* **98** 590–603
[20] Chougule A, Mann J, Kelly M, Sun J, Lenschow D H and Patton E G 2012 *J. Turbul.* **13(36)** 1–13
[21] Chougule A 2013 Influence of atmospheric stability on the spatial structure of turbulence PhD Thesis PhD-0028 (EN) The Technical University of Denmark